International Journal of Engineering & Technology, 11 (1) (2022) 50-58

International Journal of Engineering & Technology

Website: www.sciencepubco.com/index.php/IJET

Research paper

Analysis of SIW Crossover for 5G Beamforming Network Applications

Mohammed A. I. Matar[1*], Gökhan Çınar[2] and Özge Yanaz Çınar[3]

[1]*Department of Electrical and Electronics Engineering, Faculty of Engineering, Eskişehir Osmangazi University, Eskişehir, Turkey*
[2]*Department of Electrical and Electronics Engineering, Faculty of Engineering, Eskişehir Osmangazi University, Eskişehir, Turkey*
[3]*Department of Electrical and Electronics Engineering, Faculty of Engineering, Eskişehir Osmangazi University, Eskişehir, Turkey*
[*]*Corresponding author E-mail: engmatar8@gmail.com*

Abstract

A Mode-Matching Technique (MMT) with Generalized Scattering Matrix Method (GSMM) are deployed to design and analyze H-plane SIW crossover operating at 26 GHz for 5G beamforming networks applications. The introduced crossover has an 0 dB transmission over more than 4 GHz bandwidth. During the MMT formulation, the crossover structure is divided into two symmetrical cascaded parts with each part having multi-port bifurcated sections. Due to the symmetrical structure, analyzing one half of the coupler with MMT has been sufficient for full analysis. The obtained S-parameter results from MMT are compared with full-wave CST simulator results.

Keywords: *Generalized Scattering Matrix Method (GSMM), microwave crossover, Mode-Matching Technique (MMT), Substrate Integrated Waveguide (SIW), 5G beamforming.*

1. Introduction

Crossover is a four-ports important microwave component that allows two different signals from coupled ports to cross each other without mutual interferences while isolating the other two ports. It is frequently used in designing orthogonal transmission circuits such as Butler matrices and beamforming feeding networks for multi-beam antenna systems [1]. Because crossovers are used mainly in networks that have a large number of them, it is necessary to have low loss and compact crossovers [2]. Initially, crossovers were realized using three-dimensional (3D) technologies and multi-layer structures such as bond wires, underpasses, via-holes, and air-bridges [3, 4], which usually increase the fabrication complexity and the overall cost. 3D crossover designs not only introduced problems in fabrication but also exhibited non-negligible return loss in the passband [5]. Accordingly, compact and planar crossovers have been developed in recent years. However, most of these planar crossovers are mainly designed using microstrip technology, which may suffer from high losses, especially in the mm-wave region [6]. Recently, substrate integrated waveguides (SIW) have been emerged as a suitable technology to design low-losses compact circuits in microwave and mm-wave communication systems, since they have low-cost, high-quality factor, and high-power handling capability advantages. In this technology, the regular rectangular waveguide is synthesized using metallic vias inside the substrate [2].In most cases, SIW crossover structures are realized by using 0 dB directional couplers or by cascading of two 3 dB couplers [7]. In [5], dual-band SIW crossover operating at 2.4 GHz and 5.2 GHz with high port isolation is presented. In this crossover design, the dual-band propriety is achieved by utilizing the electric dipole behavior of the slots located on the bottom side of SIW structure. The 10 dB fractional bandwidth of the first pass-band is about 11.2% while the second one is about 10.9% with more than 40 dB isolation for both bands. The proposed SIW filtering crossover in [8] is designed based on the orthogonal degenerate TE_{201} and TE_{102} modes in SIW square cavities. At the cavity center, the feeding ports and also the coupling gaps are arranged to achieve good transmission and isolation responses. As a prototype based on the previous technique, narrow-band SIW crossover is designed at 20 GHz operating frequency with FBW of about 2.4% and more than 30 dB of isolation. Based on SIW and stripline techniques, the paper in [1] presents wide-band planar directional coupled crossover by integrating 3 dB stripline coupler into another 3 dB SIW coupler. In the proposed structure, since TE_{10} and TEM modes are approximately orthogonal, good transmission with high isolation can be obtained. A 26 GHz crossover prototype for 5G applications is designed and fabricated with 15.7% FBW and around 16 dB port isolation. SIW to grounded coplanar waveguide (GCPW) transition used to implement a wideband planar crossover presented in [2]. The obtained bandwidth of the designed crossover almost covers the band between TE_{10} and TE_{20} SIW modes cutoff frequencies. The proposed crossover has more than 20 dB of port isolation in the operating bandwidth which is between 9-18 GHz. In [9], two SIW filtering crossover designs with high selectivity are presented. The cross-transmission and channel isolation of

the crossovers are realized by employing the orthogonal degenerate TE_{201} and TE_{102} SIW modes in center square cavity. The proposed crossover operates at 20 GHz with about 6.6% of 3-dB FBW and around 20 dB of port isolation. Although full-wave simulators such as CST and HFSS are used generally to design,analyze and optimize the microwave components including SIW crossovers, these simulators may have some latency due to large memory occupation especially in SIW structures because of its many discontinuities [10].Therefore, numerical methods such as Mode Matching Technique (MMT) are offering good choices to implement fast and accurate tools to analyze various microwave components. Mode Matching Technique with the Generalized Scattering Matrix Method (GSMM) is successfully used in designing different microwave components that have discontinuities either physically or geometrically. This approach was applied to microstrip lines by Chu et.al [11] and Chu and Itoh [12] while in 1994, Eleftheriades et.al considered MMT with GSMM in their analyses of some horn antennas where they also presented a thorough analysis for the methodology of these techniques [13]. In [14], MMT is used to analyze SIW crossover which is formed by excitation of two orthogonal resonators having their respective zero-E-field locations in the center of the cross junction. The obtained MMT results successfully matched with CST and measured results at the operation band. The presented SIW crossover operates at 24.75 GHz with a bandwidth of about 3 GHz and better than 23 dB port isolation. In this paper, the MMT with GSMM approach is used to analyze SIW crossover at 26 GHz for 5G applications. The designed crossover has almost 0 dB transmission over more than 4 GHz of bandwidth and with a 0-degree phase at 26 GHz. Accurate results are obtained by using MMT, which include the multi-port symmetrical consideration of the structure. In SIW MMT analysis the square vias are assumed as structure discontinuities.The proposed coupler is also optimized with full-wave solver CST and the S-parameters results are compared with the obtained MMT results.

2. Theory & Design

2.1. SIW Structure

Figure 1 presents the structure of a regular SIW line, which is very similar to a dielectric-filled waveguide (DFW) structure as it is formed of two rows of cylindrical vias (waveguide walls) between metal cover plates, which are separated by a dielectric substrate. So, the E-field distribution in SIW is quite similar to the one in DFW [15]. The main three SIW design parameters are; SIW width w, metallic via diameter

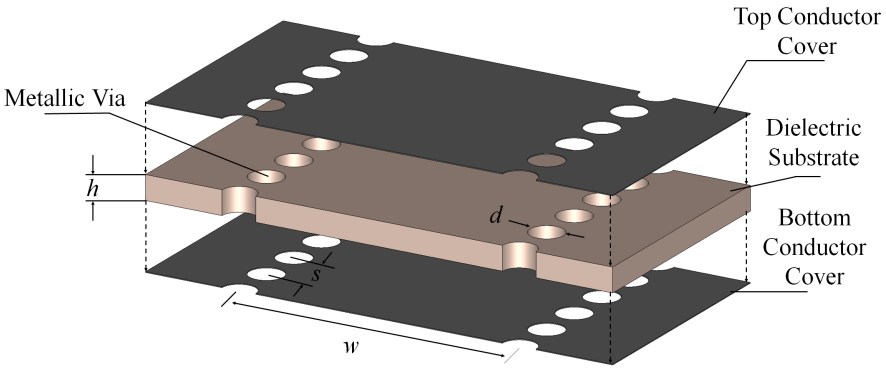

Figure 1: SIW Structure

d and the pitch s. In order to avoid any leakage from the structure, these parameters must be calculated using below formulas [16, 15]:

$$w_{eff} = w - \frac{d^2}{0.95 \times s} \tag{1}$$

$$d < \frac{\lambda_g}{5}, \quad s \leq 2d \tag{2}$$

$$\lambda_g = \frac{2\pi}{\sqrt{\frac{\varepsilon_r (2\pi f)^2}{c^2} - \left(\frac{\pi}{w}\right)}} \tag{3}$$

where, f is the frequency, λ_g is the guided wavelength and c is the speed of light. In the next subsection, SIW technology will be implemented to design hybrid SIW coupler with $d = 0.72$ mm and $s = 1$ mm

2.2. SIW Crossover Design

The designed SIW crossover structure is presented in Figure 2, which also illustrates the symmetrical dimensions of the structure. RT Duroid 5880 substrate with a relative permittivity of ε_r=2.2 and substrate height of h=508μm is used to implement this crossover. The crossover symmetrical dimensions for the frequency range of 23 GHz to 27 GHz are listed in Table **??**. The crossover structure is symmetric around x-axis and z-axis, which is the directions of wave propagation, so that,analyzing one half of the structure with MMT is enough for full GSMM analysis.

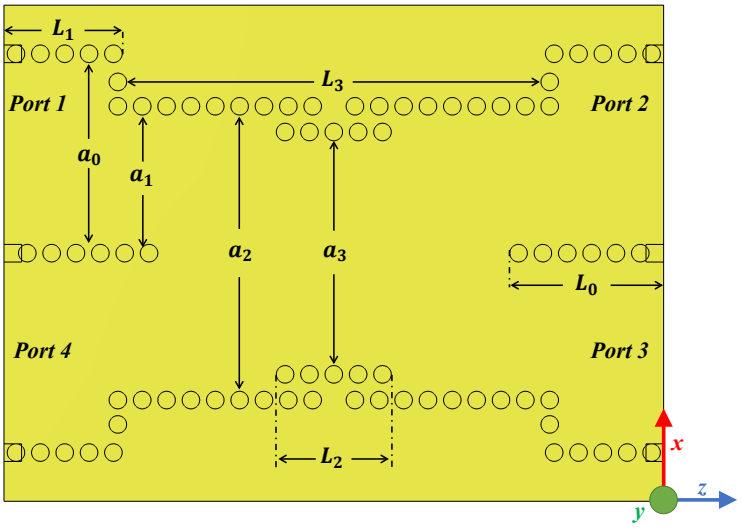

Figure 2: SIW CRossOver.

Table 1: SIW CrossOver Parameters

Parameter	mm
a_0	7.467
a_1	5.311
a_2	11.342
a_3	9.23
L_0	6.316
L_1	4.85
L_2	4.72
L_3	17.014

2.3. Mode-Matching Analysis

The designed crossover is symmetric around z-axes so that,it can be divided into two identical parts. Mode Matching Technique (MMT) is used to analyze the first half of the suggested crossover and then cascading this half with its mirror image to have the complete structure analysis. The geometrical model of the problem is presented in Figure 3. X denoting the regions I, II, III ,IV, V and VI and $k_{zm}^{(X)}$ being the wavenumber of the m-th mode propagating in the relevant region as

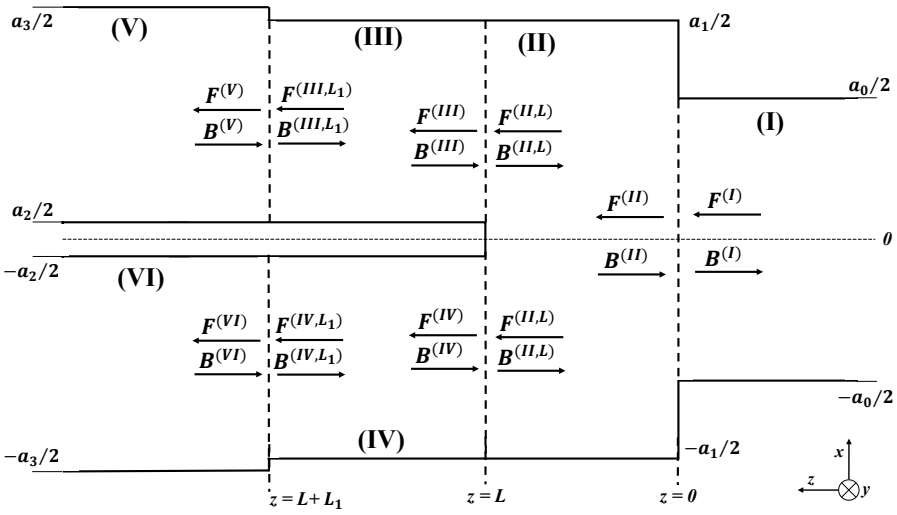

Figure 3: SIW geometrical model

$$k_{zm}^{(X)} = \begin{cases} \sqrt{\omega^2\mu\varepsilon - \left(\frac{m\pi}{b^{(X)}}\right)^2} & : \text{propagating mode} \\ -\mathrm{j}\sqrt{\left(\frac{m\pi}{b^{(X)}}\right)^2 - \omega^2\mu\varepsilon} & : \text{evanescent mode} \end{cases}, \tag{4}$$

The electric and magnetic fields in the structure regions can be described in terms of normalized modes as

$$E_y^{(X)} = \sum_{m=1}^{\infty} G_m^{(X)} \sin\left[\frac{m\pi(x+d^{(X)})}{b^{(X)}}\right] \times \left[F_m^{(X)} \mathrm{e}^{-\mathrm{j}k_{zm}^{(X)} z} + B_m^{(X)} \mathrm{e}^{\mathrm{j}k_{zm}^{(X)} z}\right] \tag{5}$$

and

$$H_x^{(X)} = -\sum_{m=1}^{\infty} G_m^{(X)} Y_m^{(X)} \sin\left[\frac{m\pi(x+d^{(X)})}{b^{(X)}}\right] \times \left[F_m^{(X)} \mathrm{e}^{-\mathrm{j}k_{zm}^{(X)} z} - B_m^{(X)} \mathrm{e}^{\mathrm{j}k_{zm}^{(X)} z}\right] \tag{6}$$

where

$$Y_m^{(X)} = \frac{k_{zm}^{(X)}}{\omega\mu}, \tag{7}$$

$$G_m^{(X)} = 2\sqrt{\frac{\omega\mu}{b^{(X)} h k_{zm}^{(X)}}}, \tag{8}$$

$$d^{(X)} = \begin{cases} a_0/2 & : X = I \\ a_1/2 & : X = II \\ -a_2/2 & : X = III \\ a_1/2 & : X = IV \\ -a_2/2 & : X = V \\ a_3/2 & : X = VI \end{cases} \tag{9}$$

and

$$b^{(X)} = \begin{cases} a_0 & : X = I \\ a_1 & : X = II \\ (a_1 - a_2)/2 & : X = III \\ (a_1 - a_2)/2 & : X = IV \\ (a_3 - a_2)/2 & : X = V \\ (a_3 - a_2)/2 & : X = V \end{cases} \tag{10}$$

At the regions boundaries, the modes are matched by considering that the tangential components of the electric and the magnetic fields are continuous. The first continuity relation at $z = 0$ which formed by regions I and II is

$$E_y^{(II)} = \begin{cases} E_y^{(I)} & : -a_0/2 \le x \le a_0/2 \\ 0 & : \text{elsewhere} \end{cases} \tag{11}$$

and

$$H_x^{(I)} = H_x^{(II)}, \quad -a_0/2 \le x \le a_0/2. \tag{12}$$

By applying these relations to the fields in equation 5 and 6, we obtain the follow

$$\begin{bmatrix} \mathbf{B^{(I)}} \\ \mathbf{F^{(II)}} \end{bmatrix} = \begin{bmatrix} \mathbf{S_{11}^{(0)}} & \mathbf{S_{12}^{(0)}} \\ \mathbf{S_{21}^{(0)}} & \mathbf{S_{22}^{(0)}} \end{bmatrix} \begin{bmatrix} \mathbf{F^{(I)}} \\ \mathbf{B^{(II)}} \end{bmatrix} \tag{13}$$

with

$$\mathbf{S_{11}^{(0)}} = \left(\mathbf{I} + \mathbf{L_H^{(0)}} \mathbf{L_E^{(0)}}\right)^{-1} \left(\mathbf{I} - \mathbf{L_H^{(0)}} \mathbf{L_E^{(0)}}\right), \tag{14}$$

$$\mathbf{S_{12}^{(0)}} = 2\left(\mathbf{I} + \mathbf{L_H^{(0)}} \mathbf{L_E^{(0)}}\right)^{-1} \mathbf{L_H^{(0)}}, \tag{15}$$

$$\mathbf{S_{21}^{(0)}} = 2\left(\mathbf{I} + \mathbf{L_E^{(0)}} \mathbf{L_H^{(0)}}\right)^{-1} \mathbf{L_E^{(0)}} = \mathbf{L_E^{(0)}}\left(\mathbf{I} + \mathbf{S_{11}^{(0)}}\right) \tag{16}$$

and

$$\mathbf{S_{22}^{(0)}} = \left(\mathbf{I} + \mathbf{L_E^{(0)}} \mathbf{L_H^{(0)}}\right)^{-1} \left(\mathbf{L_E^{(0)}} \mathbf{L_H^{(0)}} - \mathbf{I}\right) = \left(\mathbf{L_E^{(0)}} \mathbf{S_{12}^{(0)}} - \mathbf{I}\right) \tag{17}$$

Here, $\mathbf{L_E}$ and $\mathbf{L_H}$ are the coupling matrices and they are stand for the integrals

$$\left(L_E^{(0)}\right)_{mn} = 2\sqrt{\frac{k_{zm}^{(II)}}{a_0 a_1 k_{zn}^{(I)}}}\int_{-\frac{a_0}{2}}^{\frac{a_0}{2}} \sin\left(\frac{m\pi(x+a_1/2)}{a_1}\right)\times\sin\left(\frac{n\pi(x+a_0/2)}{a_0}\right)\mathrm{d}x \tag{18}$$

and

$$\left(L_H^{(0)}\right)_{mn} = \left(L_E^{(0)}\right)_{nm} \tag{19}$$

where $\mathbf{I}$ is the unit matrix. Similarly, the second continuity relations for the system formed by the regions II, III and IV at $z = L$ are

$$E_y^{(II)} = \begin{cases} E_y^{(III)} & : a_2/2 \le x \le a_1/2 \\ 0 & : -a_2/2 \le x \le a_1/2 \\ E_y^{(IV)} & : -a_1/2 \le x \le -a_2/2 \end{cases}, \tag{20}$$

$$H_x^{(III)} = H_x^{(II)},\ \ a_2/2 \le x \le a_1/2 \tag{21}$$

and

$$H_x^{(IV)} = H_x^{(II)},\ \ -a_1/2 \le x \le -a_2/2. \tag{22}$$

Substituting the fields in their relevant regions into the above relations yields

$$\begin{bmatrix} \mathbf{B^{(II,L)}} \\ \mathbf{F^{(III)}} \\ \mathbf{F^{(IV)}} \end{bmatrix} = \begin{bmatrix} \mathbf{S_{11}^{(L)}} & \mathbf{S_{12}^{(L)}} & \mathbf{S_{13}^{(L)}} \\ \mathbf{S_{21}^{(L)}} & \mathbf{S_{22}^{(L)}} & \mathbf{S_{23}^{(L)}} \\ \mathbf{S_{31}^{(L)}} & \mathbf{S_{32}^{(L)}} & \mathbf{S_{33}^{(L)}} \end{bmatrix} \begin{bmatrix} \mathbf{F^{(II,L)}} \\ \mathbf{B^{(III)}} \\ \mathbf{B^{(IV)}} \end{bmatrix} \tag{23}$$

where

$$\mathbf{S_{11}^{(L)}} = \left(\mathbf{I} + \mathbf{L_{E1}^{(L)}}\mathbf{L_{H1}^{(L)}} + \mathbf{L_{E2}^{(L)}}\mathbf{L_{H2}^{(L)}}\right)^{-1} \times \left(\mathbf{L_{E1}^{(L)}}\mathbf{L_{H1}^{(L)}} + \mathbf{L_{E2}^{(L)}}\mathbf{L_{H2}^{(L)}} - \mathbf{I}\right) \tag{24}$$

$$\mathbf{S_{12}^{(L)}} = 2\left(\mathbf{I} + \mathbf{L_{E1}^{(L)}}\mathbf{L_{H1}^{(L)}} + \mathbf{L_{E2}^{(L)}}\mathbf{L_{H2}^{(L)}}\right)^{-1}\mathbf{L_{E1}^{(L)}} \tag{25}$$

$$\mathbf{S_{13}^{(L)}} = 2\left(\mathbf{I} + \mathbf{L_{E1}^{(L)}}\mathbf{L_{H1}^{(L)}} + \mathbf{L_{E2}^{(L)}}\mathbf{L_{H2}^{(L)}}\right)^{-1}\mathbf{L_{E2}^{(L)}} \tag{26}$$

$$\mathbf{S_{21}^{(L)}} = \left(\mathbf{L_{H1}^{(L)}} - \mathbf{L_{H1}^{(L)}}\mathbf{S_{11}^{(L)}}\right) \tag{27}$$

$$\mathbf{S_{22}^{(L)}} = \left(\mathbf{I} - \mathbf{L_{H1}^{(L)}}\mathbf{S_{12}^{(L)}}\right) \tag{28}$$

$$\mathbf{S_{23}^{(L)}} = -\mathbf{L_{H1}^{(L)}}\mathbf{S_{13}^{(L)}} \tag{29}$$

$$\mathbf{S_{31}^{(L)}} = \left(\mathbf{L_{H2}^{(L)}} - \mathbf{L_{H2}^{(L)}}\mathbf{S_{11}^{(L)}}\right) \tag{30}$$

$$\mathbf{S_{32}^{(L)}} = -\mathbf{L_{H2}^{(L)}}\mathbf{S_{12}^{(L)}} \tag{31}$$

and

$$\mathbf{S_{33}^{(L)}} = \left(\mathbf{I} - \mathbf{L_{H2}^{(L)}}\mathbf{S_{13}^{(L)}}\right) \tag{32}$$

with

$$\left(L_{E1}^{(L)}\right)_{mn} = 2\sqrt{\frac{2k_{zm}^{(II)}}{a_1(a_1-a_2)k_{zn}^{(III)}}}\int_{\frac{a_2}{2}}^{\frac{a_1}{2}} \sin\left(\frac{m\pi\left(x+\frac{a_1}{2}\right)}{a_1}\right) \times\sin\left(\frac{n\pi\left(x-\frac{a_2}{2}\right)}{\frac{a_1}{2}-\frac{a_2}{2}}\right)\mathrm{d}x = \left(L_{H1}^{(L)}\right)_{nm} \tag{33}$$

and

$$\left(L_{E2}^{(L)}\right)_{mn} = 2\sqrt{\frac{2k_{zm}^{(I)}}{a_1(a_1-a_2)k_{zn}^{(IV)}}}\int_{-\frac{a_1}{2}}^{-\frac{a_2}{2}} \sin\left(\frac{m\pi\left(x+\frac{a_1}{2}\right)}{a_1}\right) \times \sin\left(\frac{n\pi\left(x+\frac{a_1}{2}\right)}{\frac{a_1}{2}-\frac{a_2}{2}}\right) = \left(L_{H2}^{(L)}\right)_{nm}. \tag{34}$$

Now, the obtained 2×2 and 3×3 matrices are cascaded by apply the generalized scattering matrix method as it is presented in Figure 3, the relations are

$$\mathbf{F^{(I,L)}} = \mathbf{DF^{(I)}} \tag{35}$$

$$\mathbf{B^{(I)}} = \mathbf{DB^{(I,L)}} \tag{36}$$

where

$$\mathbf{D} = \mathrm{diag}\left\{\mathrm{e}^{-\mathrm{j}k_{zm}^{(II)}L}\right\} \tag{37}$$

By the help of Generalized Scattering Matrix Method, 3×3 matrix is obtained as follow

$$\begin{bmatrix}\mathbf{B^{(I)}}\\ \mathbf{F^{(III)}}\\ \mathbf{F^{(IV)}}\end{bmatrix} = \begin{bmatrix}\mathbf{S_{11}^{(T)}} & \mathbf{S_{12}^{(T)}} & \mathbf{S_{13}^{(T)}}\\ \mathbf{S_{21}^{(T)}} & \mathbf{S_{22}^{(T)}} & \mathbf{S_{23}^{(T)}}\\ \mathbf{S_{31}^{(T)}} & \mathbf{S_{32}^{(T)}} & \mathbf{S_{33}^{(T)}}\end{bmatrix}\begin{bmatrix}\mathbf{F^{(I)}}\\ \mathbf{B^{(III)}}\\ \mathbf{B^{(IV)}}\end{bmatrix} \tag{38}$$

with

$$\mathbf{S_{11}} = \mathbf{S_{11}^{(0)}} + \mathbf{S_{12}^{(0)}DUS_{11}^{(L)}DS_{21}^{(0)}} \tag{39}$$

$$\mathbf{S_{12}} = \mathbf{S_{12}^{(0)}DUS_{12}^{(L)}} \tag{40}$$

$$\mathbf{S_{13}} = \mathbf{S_{12}^{(0)}DUS_{13}^{(L)}} \tag{41}$$

$$\mathbf{S_{21}} = \mathbf{S_{21}^{(L)}DVS_{21}^{(0)}} \tag{42}$$

$$\mathbf{S_{22}} = \mathbf{S_{21}^{(L)}DVS_{22}^{(0)}DS_{12}^{(L)}} + \mathbf{S_{22}^{(L)}} \tag{43}$$

$$\mathbf{S_{23}} = \mathbf{S_{21}^{(L)}DVS_{22}^{(0)}DS_{13}^{(L)}} + \mathbf{S_{23}^{(L)}} \tag{44}$$

$$\mathbf{S_{31}} = \mathbf{S_{31}^{(L)}DVS_{21}^{(0)}} \tag{45}$$

$$\mathbf{S_{32}} = \mathbf{S_{31}^{(L)}DVS_{22}^{(0)}DS_{12}^{(L)}} + \mathbf{S_{32}^{(L)}} \tag{46}$$

and

$$\mathbf{S_{33}} = \mathbf{S_{31}^{(L)}DVS_{22}^{(0)}DS_{13}^{(L)}} + \mathbf{S_{33}^{(L)}} \tag{47}$$

Here the matrices $\mathbf{U}$ and $\mathbf{V}$ stand for

$$\mathbf{U} = \left(\mathbf{I} - \mathbf{S_{11}^{(L)}DS_{22}^{(0)}D}\right)^{-1} \tag{48}$$

and

$$\mathbf{V} = \left(\mathbf{I} - \mathbf{S_{22}^{(0)}DS_{11}^{(L)}D}\right)^{-1}, \tag{49}$$

respectively. The last two continuity relations at $z = L + L_1$ formed by regions (III, V) and (IV, VI) are

$$E_y^{(V)} = \begin{cases} E_y^{(III)} & : a_2/2 \le x \le a_1/2 \\ 0 & : a_1/2 \le x \le a_3/2 \end{cases}, \tag{50}$$

$$H_x^{(III)} = H_x^{(V)}, \;\; a_2/2 \le x \le a_1/2 \tag{51}$$

and

$$E_y^{(VI)} = \begin{cases} E_y^{(IV)} & : -a_1/2 \le x \le -a_2/2 \\ 0 & : -a_3/2 \le x \le -a_1/2 \end{cases}, \tag{52}$$

$$H_x^{(IV)} = H_x^{(VI)}, \quad -a_1/2 \le x \le -a_2/2. \tag{53}$$

The scattering 2×2 matrix for the upper discontinuity can obtained using equations (13-17) as

$$\begin{bmatrix} \mathbf{B^{(III,L_1)}} \\ \mathbf{F^{(V)}} \end{bmatrix} = \begin{bmatrix} \mathbf{S_{11}^{(1)}} & \mathbf{S_{12}^{(1)}} \\ \mathbf{S_{21}^{(1)}} & \mathbf{S_{22}^{(1)}} \end{bmatrix} \begin{bmatrix} \mathbf{F^{(III,L_1)}} \\ \mathbf{B^{(V)}} \end{bmatrix} \tag{54}$$

with

$$\left(L_E^{(1)}\right)_{mn} = 2\sqrt{\frac{k_{zm}^{(V)}}{(\frac{a_1}{2}-\frac{a_2}{2})(\frac{a_3}{2}-\frac{a_2}{2})k_{zn}^{(III)}}} \int_{\frac{a_2}{2}}^{\frac{a_1}{2}} \sin\left(\frac{m\pi(x-a_2/2)}{\frac{a_3}{2}-\frac{a_2}{2}}\right) \times \sin\left(\frac{n\pi(x-a_2/2)}{\frac{a_1}{2}-\frac{a_2}{2}}\right) \mathrm{d}x \tag{55}$$

$$\left(L_H^{(1)}\right)_{mn} = \left(L_E^{(1)}\right)_{nm} \tag{56}$$

similarly for the lower discontinuity,

$$\begin{bmatrix} \mathbf{B^{(IV,L_1)}} \\ \mathbf{F^{(VI)}} \end{bmatrix} = \begin{bmatrix} \mathbf{S_{11}^{(2)}} & \mathbf{S_{12}^{(2)}} \\ \mathbf{S_{21}^{(2)}} & \mathbf{S_{22}^{(2)}} \end{bmatrix} \begin{bmatrix} \mathbf{F^{(IV,L_1)}} \\ \mathbf{B^{(VI)}} \end{bmatrix} \tag{57}$$

with

$$\left(L_E^{(2)}\right)_{mn} = 2\sqrt{\frac{k_{zm}^{(VI)}}{(\frac{a_1}{2}-\frac{a_2}{2})(\frac{a_3}{2}-\frac{a_2}{2})k_{zn}^{(IV)}}} \int_{-\frac{a_1}{2}}^{-\frac{a_2}{2}} \sin\left(\frac{m\pi(x+a_1/2)}{\frac{a_3}{2}-\frac{a_2}{2}}\right) \times \sin\left(\frac{n\pi(x+a_1/2)}{\frac{a_1}{2}-\frac{a_2}{2}}\right) \mathrm{d}x \tag{58}$$

$$\left(L_H^{(2)}\right)_{mn} = \left(L_E^{(2)}\right)_{nm} \tag{59}$$

Finally, the 3×3 scattering matrix in equation (38) is cascaded simultaneously with the obtained two 2×2 matrices in (54) and (57) by apply the generalized scattering matrix method as it is presented in Figure (3), the relations are

$$\mathbf{F^{(III,L_1)}} = \mathbf{D_1 F^{(III)}} \tag{60}$$

$$\mathbf{B^{(III)}} = \mathbf{D_1 B^{(III,L_1)}} \tag{61}$$

and

$$\mathbf{F^{(IV,L_1)}} = \mathbf{D_2 F^{(IV)}} \tag{62}$$

$$\mathbf{B^{(IV)}} = \mathbf{D_2 B^{(IV,L_1)}} \tag{63}$$

where

$$\mathbf{D_1} = \mathrm{diag}\left\{\mathrm{e}^{-\mathrm{j}k_{zm}^{(III)}L_1}\right\} \tag{64}$$

and

$$\mathbf{D_2} = \mathrm{diag}\left\{\mathrm{e}^{-\mathrm{j}k_{zm}^{(IV)}L_1}\right\} \tag{65}$$

By having the scattering matrix of one half of the crossover design, it can easily obtain the overall 4×4 scattering matrix by cascading it with its mirrored one which allows the full geometry rigorously analyzed by MMT.

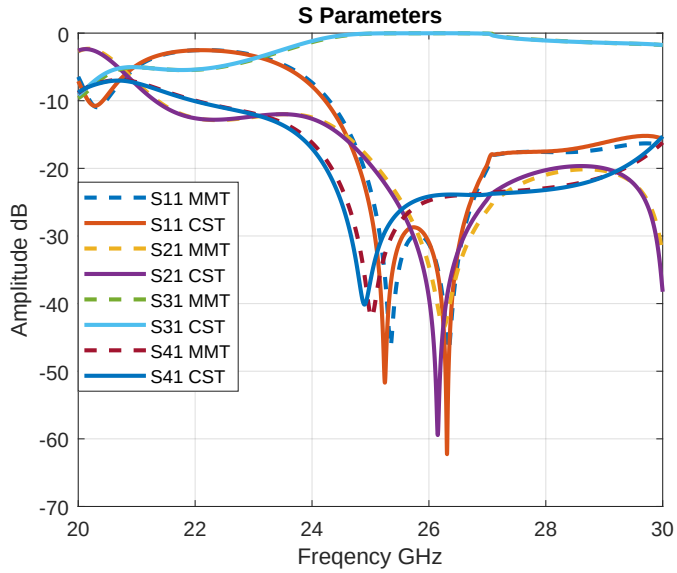

Figure 4: The crossover S Parameters

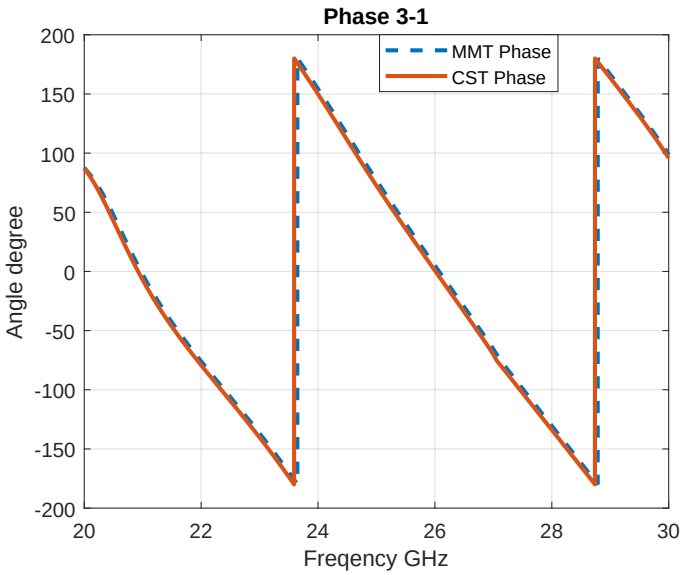

Figure 5: The phase shift between port (1) and (3)

3. Results & Discussion

This section discusses the performance the designed crossover in terms of return loss, isolation and the bandwidth of the crossover. The suggested SIW crossover structure, shown in Figure 2 is optimized using full-wave simulator (CST) and analysed by MMT and the results are compared and discussed. The S_{11} parameter defines as the reflection of the input or return loss, S_{21} and S_{41} are the isolated ports and S_{31} is the coupling port. Figure 4 presents the obtained S-parameters of the crossover form CST and MMT as well. The simulation and MMT results show that the crossover has a fractional bandwidth (FBW) of about 11.6% with respect to 26 GHz as center frequency with less than -20 dB of return loss. FBW is calculated by considering (0dB) of transmission on the transmission port (port 3).The crossover structure isolates ports (2) and (4) with more than 20dB. The discontinuity at 27 GHz appeared due to higher modes effect in the structure. Although the analysis with MMT has some structure approximations such as square vias, good results agreement between MMT and CST is achieved. In MMT MATLAB code, the truncation number for MMT analysis is chosen as 45. Higher truncation number means higher results accuracy, however for truncation numbers above 25, the differences in the results are negligable.The crossover can be feeded using microstrip line feeding port or waveguide port by adding matched taper transition. The obtained phase shift between port 1 (input) and port 3 (forward) is presented in Figure 5 with 0 degree at 26 GHz, which makes this crossover suitable to be used in Butler matrix beamformer. As the signal or power is supplied to the Port 1 (input), it was forwarded to the Port 3 (forward) and since the design is not in ideal condition,the rest of the input power is delivered to the Port 2 and Port 4 (isolated). The array of via hole acting as the boundary or wall in order to avoid leakage and to guide the electromagnetic wave. The electrical field distribution at 26 GHz is presented in Figure 6. In this figure, as the array of via hole acting as a boundary to guide the electromagnetic wave, it can be seen clearly that the input signal from port (1) interacts with metallic vias as if they are conductive wall without leakage. Since the design crossover is not in ideal condition, there is a small amount of signal passing

through port 2 and port 4 which are the isolated ports.

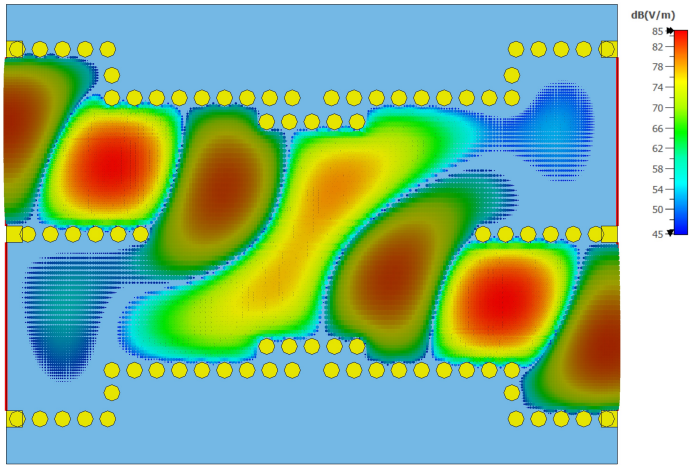

Figure 6: The electrical field distribution at 26 GHz

4. Conclusion

The analysis of 26 GHz H-plane SIW crossover with Mode-Matching Technique (MMT) and Generalized Scattering Matrix Method (GSMM) is presented. The crossover is suitable to be used in 5G beamforming networks applications.The suggested crossover has an 0 dB transmission over more than 4 GHz bandwidth with good port isolation. In MMT analysis, the crossover structure divided into two symmetrical 3-port cascaded parts with each part having multi-port bifurcated sections. MMT and GSMM formulation steps are illustrated during the paper. The obtained MMT S-parameter results introduces a good matching when compared with full-wave CST simulator results.

References

[1] Y.-Y. Cao, Y.-W. Wu, Z. Jiang, and Z.-C. Hao, "A compact millimeter-wave planar directional coupled crossover with a wide bandwidth," *IEEE Microwave and Wireless Components Letters*, vol. 30, no. 7, pp. 661–664, 2020.
[2] A. Bagheri and G. Moradi, "A wideband single-layer crossover using substrate integrated waveguide to grounded coplanar waveguide transition," *Microwave and Optical Technology Letters*, vol. 59, no. 11, pp. 2757–2762, 2017.
[3] T.-S. Horng, "A rigorous study of microstrip crossovers and their possible improvements," *IEEE Transactions on Microwave Theory and Techniques*, vol. 42, no. 9, pp. 1802–1806, 1994.
[4] T. Becks and I. Wolff, "Analysis of 3-d metallization structures by a full-wave spectral-domain technique," *IEEE Transactions on Microwave Theory and Techniques*, vol. 40, no. 12, pp. 2219–2227, 1992.
[5] S. Karthikeyan, "Compact dual-band substrate integrated waveguide crossover with high isolation," *Progress In Electromagnetics Research Letters*, vol. 38, p. 23–28, 2019.
[6] Y. Zhou, K. Zhou, J. Zhang, C. Zhou, and W. Wu, "Miniaturized substrate integrated waveguide filtering crossover," in *2017 IEEE Electrical Design of Advanced Packaging and Systems Symposium (EDAPS)*, 2017, pp. 1–3.
[7] T. Djerafi and K. Wu, "60 ghz substrate integrated waveguide crossover structure," in *2009 European Microwave Conference (EuMC)*, 2009, pp. 1014–1017.
[8] S.-Q. Han, K. Zhou, J.-D. Zhang, C.-X. Zhou, and W. Wu, "Novel substrate integrated waveguide filtering crossover using orthogonal degenerate modes," *IEEE Microwave and Wireless Components Letters*, vol. 27, no. 9, pp. 803–805, 2017.
[9] Y. Zhou, K. Zhou, J.-D. Zhang, Zhou, and W. Wu, "Substrate-integrated waveguide filtering crossovers with improved selectivity," *International Journal of RF and Microwave Computer-Aided Engineering*, vol. 30, no. 3, 2019.
[10] Z. Kordiboroujeni and J. Bornemann, "Design of substrate integrated waveguide components using mode-matching techniques," in *2015 IEEE MTT-S International Conference on Numerical Electromagnetic and Multiphysics Modeling and Optimization (NEMO)*, 2015, pp. 1–3.
[11] T. S. Chu, T. Itoh, and Y.-C. Shih, "Comparative study of mode-matching formulations for microstrip discontinuity problems," *IEEE Transactions on Microwave Theory and Techniques*, vol. 33, no. 10, pp. 1018–1023, 1985.
[12] T. S. Chu and T. Itoh, "Generalized scattering matrix method for analysis of cascaded and offset microstrip step discontinuities," *IEEE Transactions on Microwave Theory and Techniques*, vol. 34, no. 2, pp. 280–284, 1986.
[13] G. Eleftheriades, A. Omar, L. Katehi, and G. Rebeiz, "Some important properties of waveguide junction generalized scattering matrices in the context of the mode matching technique," *IEEE Transactions on Microwave Theory and Techniques*, vol. 42, no. 10, pp. 1896–1903, 1994.
[14] S. S. Hesari and J. Bornemann, "Substrate integrated waveguide crossover formed by orthogonal te102 resonators," in *2017 47th European Microwave Conference (EuMC)*, 2017, pp. 17–20.
[15] J. Wang and T. Ling, "Novel broadband design of siw directional coupler," *The Journal of Engineering*, vol. 2019, no. 20, p. 6633–6636, 2019.
[16] M. Boulesbaa, T. Djerafi, A. Bouchekhlal, and B. Mekimah, "Design of a directional coupler based on siw technology for x band applications," in *2020 1st International Conference on Communications, Control Systems and Signal Processing (CCSSP)*, 2020, pp. 85–89.